Journal of Electronics, Electromedical Engineering, and Medical Informatics
Homepage: jeeemi.org; Vol. 7, No. 3, July 2025, pp: 646-662 e-ISSN: 2656-8632

RESEARCH ARTICLE OPEN ACCESS

Comparative Analysis of Cervical Cell Classification Using Machine Learning Algorithms

Wan Azani Mustafa[1, 2], Khalis Khiruddin [1], Khairur Rijal Jamaludin[3], Firdaus Yuslan Khusairi[1], and Shahrina Ismail.[4]

[1] Faculty of Electrical Engineering & Technology, Universiti Malaysia Perlis, Pauh Putra Campus, 02600 Arau, Perlis, Malaysia
[2] Advanced Computing (AdvComp), Centre of Excellence (CoE), Universiti Malaysia Perlis (UniMAP), Campus Pauh Putra, 02600 Arau, Perlis, Malaysia
[3] Faculty of Artificial Intelligence, Universiti Teknologi Malaysia, Jalan Sultan Yahya Petra, 54100 Kuala Lumpur, Malaysia
[4] Faculty of Science and Technology, Universiti Sains Islam Malaysia (USIM), Negeri Sembilan, Bandar Baru Nilai, 71800, Malaysia

Corresponding author: Wan Azani Mustafa (e-mail: wanazani@unimap.edu.my), **Author(s) Email**: Khalis Khiruddin (e-mail: khalisdanial@studentmail.unimap.edu.my, Khairur Rijal Jamaludin (e-mail: khairur.kl@utm.my), Firdaus Yuslan Khusairi (e-mail: s201361529@studentmail.unimap.edu.my), Shahrina Ismail (e-mail: shahrinaismail@usim.edu.my)

Abstract **Cervical cancer remains a major global health issue and is the second most common cancer affecting women worldwide. Early detection is crucial for effective treatment but remains challenging due to the asymptomatic nature of the disease and the visual complexity of cervical cell structures, which are often affected by inconsistent staining, poor contrast, and overlapping cells. This study aims to classify cervical cell images using Artificial Intelligence (AI) techniques by comparing the performance of Convolutional Neural Networks (CNN), Support Vector Machine (SVM), and K-Nearest Neighbors (KNN). The Herlev Pap smear image dataset was used for experimentation. In the preprocessing phase, images were resized to 100 × 100 pixels and enhanced through grayscale conversion, Gaussian smoothing for noise reduction, contrast stretching, and intensity normalization. Segmentation was performed using region-growing and active contour methods to accurately isolate cell nuclei. All classifiers were implemented using MATLAB. Experimental results show that CNN achieved the highest performance, with an accuracy of 85%, precision of 86.7%, and sensitivity of 83%, outperforming both SVM and KNN. These findings indicate that CNN is the most effective approach for cervical cell classification in this study. However, limitations such as class imbalance and occasional segmentation inconsistencies impacted overall performance, particularly in detecting abnormal cells. Future work will focus on improving classification accuracy—especially for abnormal samples—by exploring data augmentation techniques such as Generative Adversarial Networks (GANs) and implementing ensemble learning strategies. Additionally, integrating the proposed system into a real-time diagnostic platform using a graphical user interface (GUI) could support clinical decision-making and enhance cervical cancer screening programs.**

Keywords **Cervical cell classification; Convolutional Neural Network; Image segmentation; Support Vector Machine; K Nearest Neighbours**.

1. Introduction

Cervical cancer is a significant illness that poses a serious threat to women's health. It is acknowledged as the second most common and deadly cancer affecting women globally [1]. This cancer arises when the skin and mucosal cells in the cervical and vaginal areas become infected over time, often due to persistent infection with high-risk human papillomavirus (HPV) strains [2]. The most concerning aspect of this malignancy is that it often does not exhibit symptoms in its early stages, making early detection crucial for effective treatment [3].

Manuscript received March 20, 2025; Accepted May 12, 2025; date of publication May 20, 2025
Digital Object Identifier (**DOI**): https://doi.org/10.35882/jeeemi.v7i2.652

To address this issue, researchers aim to enhance the speed and precision of detecting and classifying various cervical cell types, particularly abnormal cells with different levels of abnormalities [4]. The task, however, is challenging due to variations in image quality, overlapping cells, artifacts, and large datasets. Ensuring robustness against noise, inter-patient variability, and other inconsistencies remains a significant hurdle [5].This study tackles the limitations of inaccurate and unreliable cervical cell image classification methods. Many current approaches face challenges with high false-positive and false-negative rates, leading to the misclassification of normal and abnormal cells, which can cause patient anxiety or delay timely interventions [6]. The complexity of cervical cell images, with diverse cell types, irregular shapes, and varying staining patterns, further complicates classification tasks [7].

Additionally, imbalanced datasets exacerbate the problem, often resulting in biased models that perform well on majority classes but poorly on minority classes [8]. Another critical issue arises from intricate cell structures affected by inconsistent staining, poor contrast, and overlapping cells, which hinder the accurate identification of individual cells and their features [9]. Effective segmentation and classification techniques are thus essential for accurate cervical cancer screening and diagnosis.

Over the years, several studies have proposed different methods to enhance segmentation accuracy and classification performance. Rasheed et al. [10] proposed an advanced UNet architecture that enhanced boundary localization and minimized errors in overlapping cell segmentation. However, the model's robustness was impacted by noise and artifacts in some images. Zhang et al. [11] enhanced segmentation performance by incorporating a global context mechanism into the traditional UNet (GC-UNet), which improved the delineation of nuclei and effectively handled overlapping cells. Despite these advancements, background noise and inconsistent contrast in some Pap smear images remained challenging. Ji et al. [12] introduced a deep ensemble learning approach by integrating multiple CNN-based models, which reduced false positives and enhanced nucleus detection. However, the increased computational complexity limited its scalability for real-time applications. Wubineh et al. [13] proposed a RES_DCGAN-based data augmentation technique combined with a self-attention-enhanced ResNet50V2 for cervical cell classification. While this approach improved feature extraction and addressed data scarcity, it did not focus on segmentation challenges like overlapping cells and inconsistent staining. Zhang et al. [14] proposed a time-series-based detection approach that analyzed smear image sequences to detect cellular changes over time, significantly improving detection accuracy. However, the reliance on temporal data limited its applicability in setups lacking access to such sequences.

Nanni et al. [15] enhanced classification accuracy by combining deep CNN features with handcrafted features and SVM classifiers. Wu et al. [16] improved performance with a hybrid CNN-LSVM model optimized using Adaboost, achieving 99.5% classification accuracy. Mustafa et al. [17] leveraged transfer learning by fine-tuning ResNet-50 and GoogLeNet models, demonstrating superior accuracy even on small datasets. However, CNN-based methods typically require large labeled datasets and significant computational resources, which can limit their deployment in resource-constrained environments [18]. Ghoneim et al. [19] developed a CNN-ELM ensemble that combined deep and shallow learning models, achieving 99.5% accuracy while reducing training time. Conceição et al. [20] integrated Random Forest (RF) with Gradient Boosting Trees (GBT), improving noise robustness and classification performance. Mohammed et al. [21] designed an ensemble model combining CNNs, Decision Trees, and k-NN classifiers, achieving high sensitivity and specificity.

Mansoury et al. [22] further enhanced ELMs by integrating genetic algorithms for parameter optimization, improving classification performance. Wei et al. [23] employed texture-based feature extraction and k-NN, achieving competitive performance on benchmark Pap smear datasets. Chaabane et al. [24] enhanced Decision Tree classifiers using bagging and boosting techniques, reducing variance and bias. However, k-NN can be computationally intensive due to distance-based calculations, while Decision Trees are prone to overfitting, particularly when applied to noisy data [25]

These studies demonstrate progress in cervical cell segmentation and classification; however, several gaps remain. Many approaches treat segmentation and classification as separate tasks, which can limit overall system performance, and challenges such as noisy data and inconsistent staining are still not fully addressed.

This research uniquely integrates dual segmentation techniques—region growing and active contours—with a comparative analysis of three classifiers (CNN, SVM, and KNN) on the same segmented data, providing a comprehensive evaluation under consistent preprocessing conditions. The CNN model is specifically designed as a lightweight, standalone architecture optimized for computational efficiency, making it suitable for resource-constrained clinical settings where rapid, automated screening is essential.

Manuscript received March 20, 2025; Accepted May 12, 2025; date of publication May 20, 2025
Digital Object Identifier (**DOI**): https://doi.org/10.35882/jeeemi.v7i2.652

The classifiers selected offer distinct strengths: CNNs, as deep learning architectures, automatically extract hierarchical features and effectively capture spatial relationships in complex cervical cell images [26]. SVMs perform well in high-dimensional spaces, handling non-linear boundaries robustly [27]. KNN, a simple yet powerful instance-based method, is effective for irregular decision boundaries [5]. Our main contributions are:

1. A combined preprocessing pipeline (Gaussian smoothing, contrast stretching, intensity normalization) tailored to improve image quality for cervical cell analysis.
2. A dual segmentation approach focusing on precise nucleus detection, which is critical for accurate classification but often overlooked in isolation.
3. A thorough comparative evaluation of CNN, SVM, and KNN classifiers applied to uniformly segmented images, highlighting trade-offs between accuracy, complexity, and practicality.

By addressing segmentation and classification jointly and optimizing for real-world clinical constraints, this study offers a more integrated and practical solution for automated cervical cell analysis. This study is structured as follows: Section 2 outlines the dataset utilized and the proposed methods for segmentation, post-processing, feature extraction, and classification. Section 3 presents the classification results. Section 4 provides an in-depth interpretation of the results, categorized and compared accordingly. Lastly, Section 5 summarizes the main findings in the conclusions.

2. Method

In this study, there are several image-processing techniques will be applied to be able to classify the image into normal and abnormal. In this study, to classify the cervical cell images, the system has to detect the cells that have been processed by image processing. The procedures for developing image processing steps for the process for classifying cervical cell images with the help of Artificial Intelligence (AI) is illustrated in Fig. 1.

Based on Fig. 1, the categorization of cervical cell images using AI consists of steps that need to be done, such as research and study on the previous research and data acquisition. Next is the process of preprocessing to enhance the images, segmentation to extract cells and background, post-processing to remove small noise in images, feature extraction to differentiate between normal, intermediate, and abnormal, and classification to classify the images.

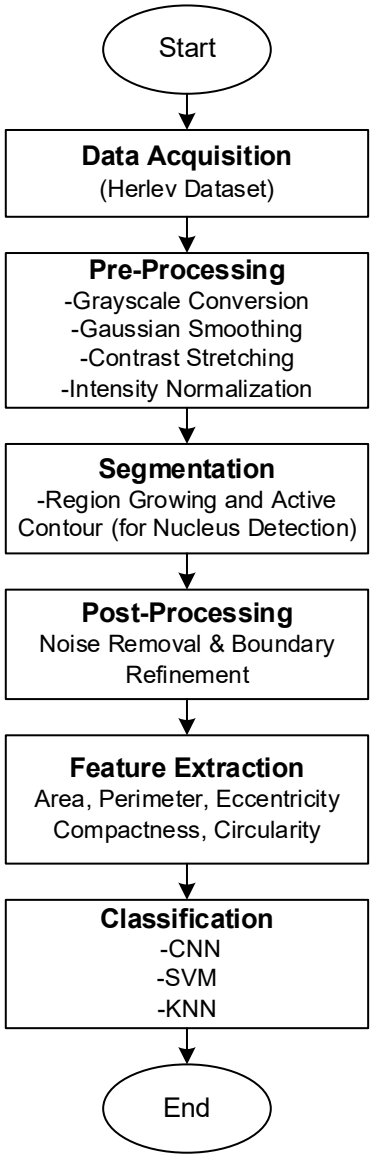

Fig. 1. Flow of Classification of Cervical Cell Image Using Machine Learning.

A. Data Acquisition

In this research, the dataset used is the publicly available Herlev database, developed at Herlev University Hospital in Denmark. The database falls under the NiSIS (Nature-Inspired Smart Information Systems, EU coordination action, contract 13569), and is accessible online at https://mde-lab.aegean.gr/index.php/downloads/. The dataset comprises 917 cervical cell images categorized into three classes: normal, intermediate, and abnormal. As shown in Fig. 2, normal cells typically exhibit a small, round or oval nucleus with a relatively large cytoplasmic area. Intermediate cells present slightly enlarged, regular-shaped nuclei, while abnormal cells display

Manuscript received March 20, 2025; Accepted May 12, 2025; date of publication May 20, 2025
Digital Object Identifier (**DOI**): https://doi.org/10.35882/jeeemi.v7i2.652

irregular nuclei with distorted cytoplasm and a high nucleus-to-cytoplasm ratio.

Table 1 provides a summary of the visual attributes and image distribution across the three categories. A key issue with the dataset is class imbalance, as intermediate cells are overrepresented compared to normal and abnormal cells. To address this, data augmentation techniques including image rotation, flipping, and scaling were applied to underrepresented classes during classification, improving generalization and reducing potential bias in model training.

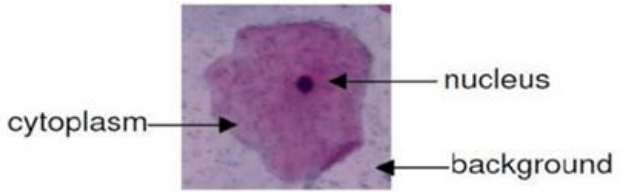

Fig. 2. The image of single cervical cell containing cytoplasm, nucleus and background from pap smear slide.

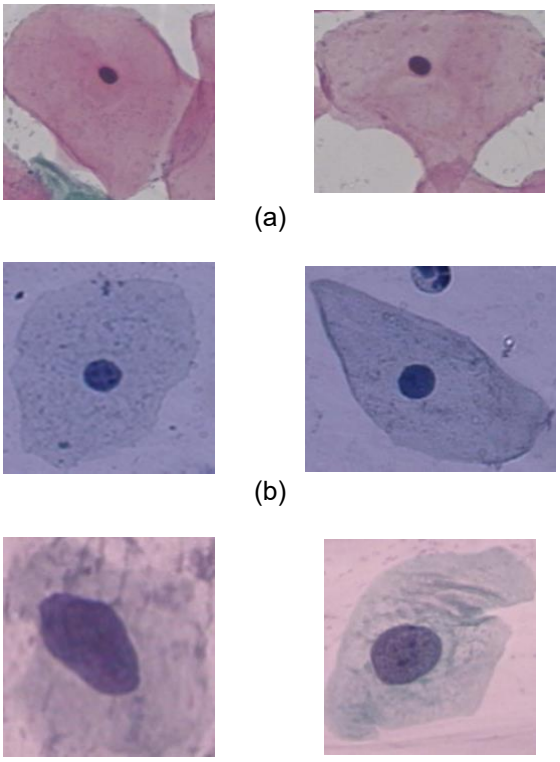

Fig. 3. The difference between the three stages of cervical cell image in term of nucleus size, cell shape and colour: (a) Normal cervical cell, (b) Intermediate cervical cell, (c) Abnormal cervical cell

Table 1. Summary of dataset distribution and visual characteristics

Class	Visual Attributes	Number of Images
Normal	Small nucleus, round/oval shape	242
Intermediate	Slightly enlarged nucleus, round/oval	525
Abnormal	Irregular shape, large nucleus, distorted cytoplasm	150
Total		**917**

B. Preprocessing Method

In the preprocessing phase, two primary techniques, image resizing and image enhancement, are implemented to improve the uniformity and quality of cervical cell images. Image resizing modifies the dimensions of input images while preserving the aspect ratio to prevent geometric distortion. In this research, all cervical cell images are resized to 100 × 100 pixels. Image enhancement is employed to improve image clarity and reduce noise, where grayscale conversion precedes the enhancement steps. Gaussian smoothing, with a standard deviation (σ) of 1.6, is applied to reduce high-frequency noise by filtering local pixel variations. This technique smooths the image by convolving it with a Gaussian function, which has proven to be effective in preprocessing cervical cytology images. For instance, in [26], a Gaussian filter was used to enhance grayscale Pap smear images and improve nuclei segmentation accuracy. Similarly, [27] employed a 3 × 3 Gaussian filter to smooth Pap smear images, enhancing subsequent classification and segmentation processes. In [28], a Laplacian of Gaussian (LoG) filter, a variant of Gaussian-based smoothing, was applied to detect and segment cervical cell nuclei with improved precision. Another study [29] demonstrated that Gaussian smoothing effectively enhances cervical cytology images prior to edge detection, contributing to better cervical cancer detection. This technique smooths the image by convolving it with a Gaussian function, expressed as Eq. (1) [29]:

$$G(x,y) = \frac{1}{2\pi\sigma^2} exp\left(-\frac{x^2+y^2}{\sigma^2}\right) \quad (1)$$

Following noise reduction, contrast stretching is applied to improve image brightness and contrast. The intensity transformation is defined by Eq. (2), which is a standard min-max normalization technique commonly used in image enhancement [30]:

Manuscript received March 20, 2025; Accepted May 12, 2025; date of publication May 20, 2025
Digital Object Identifier (**DOI**): https://doi.org/10.35882/jeeemi.v7i2.652

$$I_{new} = \frac{I_{old} - I_{min}}{I_{max} - I_{min}} \cdot \left(I_{max_{des}} - I_{min_{des}}\right) + I_{min_{des}} \quad (2)$$

where I_{old} represents the input pixel intensity, I_{min} and I_{max} are the minimum and maximum intensities of the original image, and $I_{min_{des}}$ and $I_{max_{des}}$ define the new intensity range, set between 0.1 and 1 in this work. This step enhances the overall contrast, making the cellular structures more distinguishable. Finally, intensity normalization is performed to standardize the pixel intensity distribution across images. This can be mathematically represented by Eq. (3) [30]:

$$I_{normalized} = \frac{I - \mu}{\sigma} \quad (3)$$

where I is the pixel intensity, and μ and σ are the mean and standard deviation of the pixel intensity values, respectively. These preprocessing operations, applied systematically, result in a consistent, noise-reduced, and visually enhanced dataset, facilitating improved performance in downstream cervical cell image classification tasks. The results of the image after preprocessing are depicted in Fig. 4.

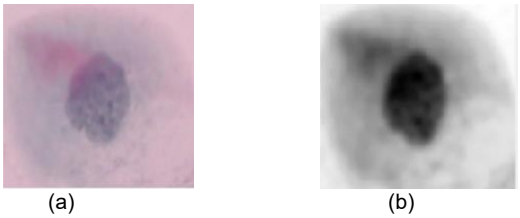

(a) (b)

Fig. 4. The result of the image after preprocessing where (a) is the original image and (b) is the result of denoise filtered image.

C. Segmentation Method

The segmentation of cervical cell images involves two key processes: the region-growing method and the active contour method. Region growing is an image processing technique that segments an image into coherent regions based on specific criteria. This method has been effectively utilized in cervical cytology image analysis. For example, Plissiti et al. applied region growing to segment cervical cell nuclei in high-resolution microscopic images, demonstrating its ability to delineate nuclear boundaries accurately and improve overall segmentation performance [31]. It starts with an initial seed point, denoted as $S_0(x_0, y_0)$ and iteratively evaluates the neighboring pixels. A pixel $p(x, y)$ is added to the growing region *R* if it satisfies a predefined condition, typically based on intensity similarity or texture consistency:

$$|I(p) - I(S_0)| < T \quad (4)$$

where $I(p)$ and $I(S_0)$ represent the intensity values of the pixel p and the seed point S_0, respectively, and T is the threshold value that controls the homogeneity of the segmented region. This iterative expansion forms a segmented region *R*, where the combined rows, columns, and adjusted threshold values define the new binary image $R(x, y)$, highlighting the segmented cervical cell area.

To enhance segmentation accuracy, particularly for nucleus detection, the active contour method (commonly known as snakes) is applied. Bamford and Lovell employed active contours in an unsupervised cell nucleus segmentation approach, achieving precise boundary detection in cervical cytology images [32]. This method seeks to minimize an energy function E as shown in Eq. (5) [32], which consists of internal energy $E_{internal}$, controlling the smoothness of the contour, and external energy $E_{external}$, which attracts the contour toward the object boundaries:

$$E = \int_0^1 \left[E_{internal}\left(v(s)\right) + E_{external}\left(v(s)\right)\right] ds \quad (5)$$

Here, $v(s) = (\mathrm{x}(\mathrm{s}), \mathrm{y}(\mathrm{s}))$ represents the parametric curve (snake) in the image domain, and $s \in [0,1]$ is the curve parameter. The internal energy can be expressed as in Eq. (6) [32]:

$$E_{internal} = \frac{\alpha}{2}\left|\frac{\partial v}{\partial s}\right|^2 + \frac{\beta}{2}\left|\frac{\partial^2}{\partial s^2}\right|^2 \quad (6)$$

where α controls the elasticity (to prevent excessive stretching), and β controls the bending (to avoid sharp corners). The external energy, $E_{external}$ as shown in Eq. (7), attracts the contour toward image features, typically based on gradients:

$$E_{external} = -|\nabla I(x, y)| \quad (7)$$

where $\nabla I(x, y)$ is the image gradient that defines the boundaries of the nucleus. The active contour iteratively deforms until it converges to the cell nucleus boundary, yielding accurate segmentation.

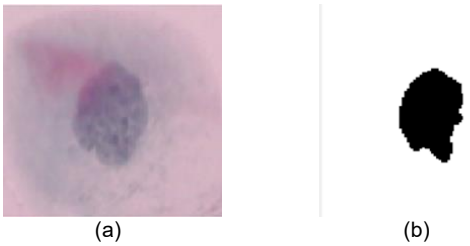

(a) (b)

Fig. 5. The result of the image after segmentation image: (a) Original Image, (b) Segmented Image

These combined segmentation techniques produce a refined binary image that highlights both the segmented cytoplasm and the detected nucleus, as shown in Fig. 5. By leveraging the region-growing method's adaptability

Manuscript received March 20, 2025; Accepted May 12, 2025; date of publication May 20, 2025
Digital Object Identifier (**DOI**): https://doi.org/10.35882/jeeemi.v7i2.652

and the active contour method's boundary precision, the segmentation process effectively delineates cervical cell structures for subsequent analysis and classification.

D. Post-Processing Method

In post-processing cervical cell images, four key morphological operations referring to [30] are undertaken to refine the binary mask $M(x,y)$ and enhance segmentation accuracy. These steps address noise, smooth region boundaries, and generate a final masked image.

1. Dilation: This operation expands the boundaries of segmented regions to connect nearby regions that may have been separated by noise. Mathematically, the dilation M_d of the binary mask MMM using a structuring element B is defined as Eq. (8):

$$M_d(x,y) = \max_{(i,j)\in B}\{M(x-i,y-j\} \quad (8)$$

   Here, the structuring element B determines the extent of dilation, which helps in merging disconnected but spatially close regions.

2. Erosion: After dilation, erosion M_e is applied to contract the boundaries of the regions, remove small noise components, and refine the shape of the segmented areas. Erosion is mathematically represented as Eq. (9):

$$M_e(x,y) = \max_{(i,j)\in B}\{M_d(x+i,y+j\} \quad (9)$$

   This step complements dilation by smoothing irregularities introduced during the expansion phase.

3. Hole Filling: The next step involves filling holes within the segmented regions. Given a binary mask M_e, the hole-filling operation can be modeled using morphological reconstruction. Let M_{hole} be the mask with filled holes. This operation can be expressed as finding the connected complement regions and filling them:

$$M_{hole} = \neg|Reconstruct(\neg M_e)| \quad (10)$$

   where ¬ denotes the complement of the mask, and the reconstruction ensures that gaps inside segmented objects are filled.

4. Masking: Finally, the refined binary mask M_{hole} is applied to the original grayscale image $I(x,y)$, preserving the intensity values within the mask's regions and setting the pixel values outside the mask to zero. This operation can be modeled as Eq. (11):

$$I_{masked}(x,y) = \begin{cases} I(x,y), if\ M_{hole}(x,y) = 1 \\ 0, if\ M_{hole}(x,y) = 0 \end{cases} \quad (11)$$

This masking step effectively removes background regions, retaining only the relevant cervical cell areas.

In summary, these post-processing steps dilation, erosion, hole filling, and masking enhance the segmentation by refining region boundaries, eliminating noise, and filling internal gaps. The final result is a clean and smooth binary mask used to generate a segmented version of the original image. The image outcome after the complete segmentation and post-processing pipeline is illustrated in Fig. 6.

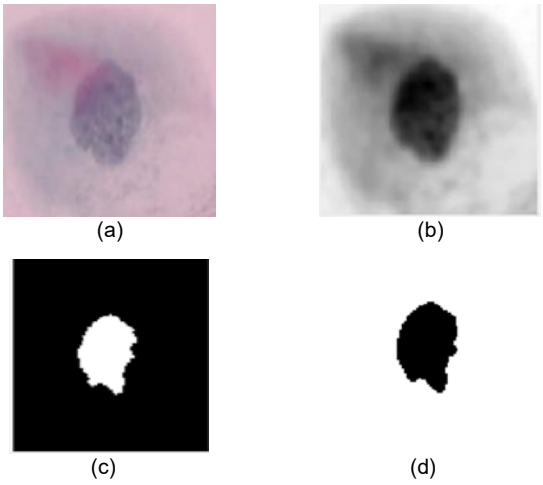

Fig. 6. Results of the image after applying the complete framework: (a) original image, (b) preprocessing, (c) region growing post-processing, and (d) segmentation.

E. Feature Extraction Method

Feature extraction focuses on shape-based features derived from the geometric properties of cervical cells. Features such as area, perimeter, eccentricity, and other shape descriptors offer insights into cell morphology. The process begins by extracting boundaries of connected components in the binary image, representing the contours of individual objects. Matrices are initialized to store shape-based features like area, perimeter, compactness, circularity, and eccentricity for each object, which are standard morphological descriptors in image analysis [30] as shown in Eq. (12) – (15). The system calculates these features for each object by extracting its boundary and determining its area, representing the total pixels enclosed. The final step involves displaying the calculated values for area, perimeter, compactness, circularity, and eccentricity. This feature extraction method provides valuable information about the

Manuscript received March 20, 2025; Accepted May 12, 2025; date of publication May 20, 2025
Digital Object Identifier (**DOI**): https://doi.org/10.35882/jeeemi.v7i2.652

morphology and structure of cervical cells. To calculate the area of cervical cells is:

$$Area = \sum_{i}^{n}\sum_{j}^{m} B(i,j), \quad (12)$$

where $B(i,j)$ is a binary image with values indicating the presence or absence of the object. To calculate the compactness:

$$Compactness = \frac{Perimeter^2}{Area}. \quad (13)$$

To calculate the circularity,

$$Circularity = \frac{4\pi Area}{Perimeter^2}. \quad (14)$$

To calculate the eccentricity,

$$Eccentricity = \sqrt{1 - \frac{b^2}{a^2}}. \quad (15)$$

E. Classification

This study employs three machine learning classifiers Convolutional Neural Network (CNN), Support Vector Machine (SVM), and K-Nearest Neighbors (KNN) each selected based on specific strengths suited to the nature of cervical cell image data. CNN is chosen for its ability to automatically learn hierarchical and spatial features from images, which is particularly advantageous given the complex morphology and variability in cervical cell structures. SVM is included for its effectiveness in high-dimensional spaces and its strong performance with small to moderately sized datasets, making it suitable for medical imaging tasks where data is often limited. KNN, a simple yet interpretable algorithm, serves as a useful baseline for comparison due to its instance-based nature and minimal training time. Although more advanced models such as ensemble deep learning or transformer-based architectures may offer higher accuracy, this study prioritizes models that balance performance with interpretability and computational efficiency. This consideration is essential for practical implementation in resource-constrained environments such as low-cost screening systems. The inclusion of these three classifiers allows for a comprehensive evaluation of model performance across different algorithmic paradigms deep learning, margin-based learning, and instance-based learning.

1) K-Nearest Neighbours

The K-Nearest Neighbours (KNN) algorithm is one of the simplest yet effective machine learning algorithms used for classification tasks, including image classification. It operates based on the principle of similarity: objects that are closer in the feature space are more likely to belong to the same category [33]. KNN is a non-parametric, instance-based learning algorithm, which means it does not make any assumptions about the underlying data distribution and memorizes the training dataset instead of learning explicit decision boundaries.

In KNN, the classification of a new input image is determined by finding its k nearest neighbours in the training dataset and assigning the label that is most frequent among these neighbours [34]. The process involves calculating the distance between the input image and each image in the training dataset. Common distance metrics used include Euclidean distance, Manhattan distance, and Minkowski distance. The most widely used distance metric, Euclidean distance, can be calculated as Eq. (16) below [35]:

$$d(x,x_i) = \sqrt{\sum_{j=1}^{n}\left(x_j - x_{i,j}\right)^2} \quad (16)$$

Here, $d(x,x_i)$ represents the Euclidean distance between the input vector *x* and a training sample x_i, where x_j and $x_{i,j}$ are the *j*-th features of *x* and x_i, respectively, and *n* is the total number of features.

In this study, the K-Nearest Neighbors (KNN) algorithm was utilized as a baseline classifier to evaluate the effectiveness of morphological features extracted from segmented cervical cell images. KNN was selected due to its intuitive, non-parametric nature and its ability to perform well on small-to-medium-sized datasets without requiring extensive model training. This study uses KNN to classify cells based on shape-based features such as area, perimeter, circularity, and eccentricity, which are relevant indicators of nucleus morphology. To optimize the performance of the classifier, several parameters were configured, including the number of neighbors (k), the distance metric, and the weighting function. The selection of these parameters was based on empirical testing and cross-validation to ensure a balanced trade-off between classification accuracy and computational efficiency. The parameters and their configurations are summarized in Table 2.

Table 2. KNN classifier parameters and configurations

Parameter	Value
k (Neighbors)	5
Distance Metric	Euclidean
Weight Function	Uniform
Feature Space	Shape-based

2) Support Vector Machine

In this research, the Support Vector Machine (SVM) algorithm is recognized as a powerful classification model within machine learning and a widely used discriminant method [36]. Compared to other

Manuscript received March 20, 2025; Accepted May 12, 2025; date of publication May 20, 2025
Digital Object Identifier (**DOI**): https://doi.org/10.35882/jeeemi.v7i2.652

classification techniques in data mining, SVM demonstrates superior generalization performance [37], [38]. It also offers advanced theoretical methods for handling non-linearly separable data. For linearly separable data, the primary objective is to identify the hyperplane that maximizes the margin, defined as the largest sum of distances between neighbouring data points and the separating line. When dealing with non-linearly separable data, SVM employs a kernel function to map the data into a higher-dimensional space, making it linearly separable [39].

SVM is specifically designed for two primary cases: linearly separable and linearly non-separable data. For linearly separable data, SVM finds the optimal hyperplane by maximizing the margin between the two classes. The discriminant function for binary classification can be expressed as Eq. (17) [39]:

$$g(x) = w^T x + b \quad (17)$$

where $g(x) = 0$ represents the hyperplane HHH, which separates the two classes. Based on this, the classification rules follow the logic outlined in Eq. (18) [39]:

$$y_i(w^T x_i +) \geq 1. \quad (18)$$

For linearly non-separable data, SVM applies a kernel function to map the input data from a lower-dimensional space to a higher-dimensional space, where the data might become linearly separable. The key mathematical operations involved in SVM classification are performed using inner products. To enhance the feature mapping, these inner product operations are replaced with kernel functions [40]. There are currently three main types of kernel functions, as expressed in the following Eq. (19) – (21) [40]:

1. Polynomial kernel function

$$K_{ploy}(x, x_i) = [(x \cdot x_i) + 1]^1 \quad (19)$$

The result is a polynomial classifier of order q;

2. Radial basis kernel function (RBF)

$$K_{ebf}(x, x_i) = exp\left(\frac{|x - x_i|^2}{\sigma^2}\right) \quad (20)$$

3. Sigmoid kernel function

$$K(x, x_i) = \tanh(v(x \cdot x_i) + c) \quad (21)$$

Different kernel functions are selected based on the specific classification problem. Among them, radial basis kernel functions and polynomial kernel functions are the most commonly used due to their strong classification capabilities. The effectiveness of SVM depends not only on selecting an appropriate kernel function but also on tuning parameter values, which directly impact the classification results. The kernel function essentially performs a mapping from a low-dimensional feature space to a higher-dimensional space, where non-linearly separable data might become linearly separable. This allows SVM to address the challenges posed by non-linear data distributions by transforming the problem into one that can be solved using linear separation techniques.

To ensure optimal classification performance, several key parameters were configured, including the choice of kernel function, regularization parameter (C), kernel coefficient (γ), and decision function shape. These parameters were selected based on empirical tuning using cross-validation to balance bias-variance trade-offs and to maximize classification accuracy. The selected parameters and their configuration space are presented in Table 3.

Table 3. SVM classifier parameters and configurations

Parameter	Value
Kernel Function	RBF
Regularization Parameter (C)	1.0
Kernel Coefficient (γ)	0.01
Tolerance (tol)	0.001

3) Convolutional Neural Network

A Convolutional Neural Network (CNN) is a specialized type of neural network, widely utilized in the field of image recognition [41], [42]. The structure of a CNN typically comprises an input layer, two convolutional layers, two pooling layers, two fully connected layers, and an output layer, making up a total of eight layers [43]. Let the *m-th* input feature map to the convolutional layer be denoted as X_m, and $W_{n,m}$ represent the convolution kernel connecting the *m-th* input feature map to the *n*-th feature map in the current layer. The output y_n of the *n-th* feature map in the convolutional layer can then be expressed as Eq. (22) [43]:

$$y_n = f\left(\sum_m X_m * W_{n,m} + b_n\right) \quad (22)$$

Here, b_n represents the bias parameter of the *n*-th feature map in the current layer, and $*$ denotes the discrete convolution operation. The function f is the activation function, commonly a non-linear mapping [16].

Pooling operations, which include max pooling and average pooling, are essential components of CNNs, helping reduce the spatial dimensions of feature maps to mitigate overfitting and enhance optimization efficiency [44]. After convolution operations extract relevant features, these features can be used to train the classifier. One common classifier is the Softmax classifier, though it can face challenges related to computational complexity.

Manuscript received March 20, 2025; Accepted May 12, 2025; date of publication May 20, 2025
Digital Object Identifier (**DOI**): https://doi.org/10.35882/jeeemi.v7i2.652

If the image input to the pooling layer is denoted as $x^{(l-1)}$, and the image output after pooling is $x^{(l)}$, the pooling operation can be represented mathematically as Eq. (23) [43], [44]:

$$x^{(l)} = dowm\left(x^{(l-1)}\right) \quad (23)$$

The fully connected layer is at the tail of the convolutional neural network. It converts the two-dimensional feature map of the convolution output into a one-dimensional vector, that is, connects all the features, and finally sends the output value to the classifier, such as Softmax classifier [45]. After Softmax, the output can be expressed as Eq. (24):

$$S(y)_i = \frac{e^{yi}}{\sum_{j=1}^{n} e^{yi}} \quad (24)$$

To enhance learning performance and prevent overfitting, several key hyperparameters were configured, including the number of convolutional filters, kernel size, activation function, optimizer type, batch size, and number of epochs. These parameters were empirically tuned based on validation performance and are summarized in Table 4.

Table 4. CNN classifier parameters and configurations

Parameter	Value
Input Image Size	100 × 100
Pooling Type	Max Pooling
Activation Function	ReLU
Optimizer	Adam
Learning Rate	0.001
Epochs	50
Loss Function	Categorical Cross-Entropy
Output Layer Activation	Softmax

The dataset was partitioned into 80% for training and 20% for testing to enable the model to learn representative patterns from the majority of the data while reserving an independent subset for unbiased performance evaluation. Due to the inherent class imbalance where intermediate-class images significantly outnumber normal and abnormal classes data augmentation was applied during the training phase to mitigate potential model bias toward the majority class. Augmentation techniques included geometric transformations such as random rotation (±15°), horizontal and vertical flipping, and random scaling within a defined range. These transformations were selectively applied to the minority classes (normal and abnormal) to synthetically increase their sample diversity and improve class balance during model training. This approach enhances the generalization capability of the classifiers, particularly for underrepresented cervical cell categories.

3. Result

In this section, 11 randomly selected images to demonstrate the performance of this system. The system contains the original images, image processing, and classification results. The segmentation results, as displayed in Fig. 7 (a)-(k), generally demonstrate the ability of the segmentation algorithm to focus on the nucleus region, which is critical for cervical cell analysis. Since the nucleus plays a significant role in distinguishing normal and abnormal cells, the primary evaluation question is how effectively the segmentation isolates and captures the nucleus across various images.

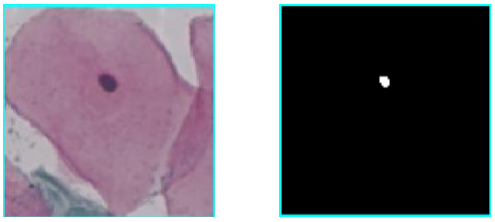

(a) Normal Superficial 10

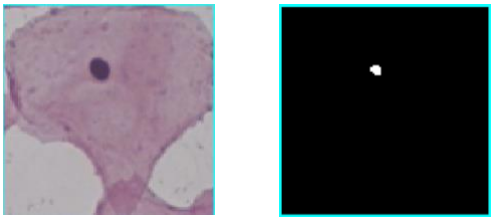

(b) Normal Superficial 11

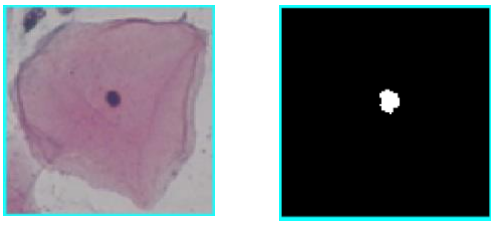

(c) Normal Superficial 29

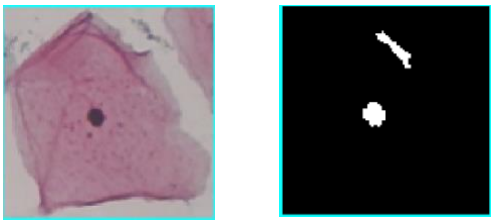

(d) Normal Superficial 47

Manuscript received March 20, 2025; Accepted May 12, 2025; date of publication May 20, 2025
Digital Object Identifier (**DOI**): https://doi.org/10.35882/jeeemi.v7i2.652

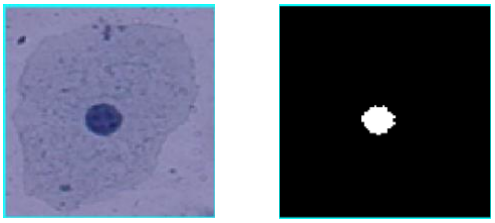

(e) Intermediate 21

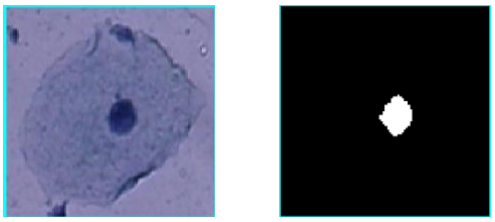

(f) Intermediate 3

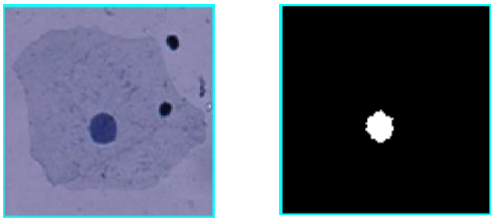

(g) Intermediate 121

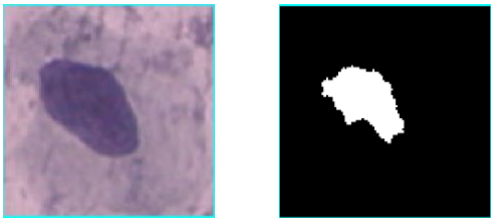

(h) Abnormal 3

(i) Abnormal 41

(j) Abnormal 102

(k) Abnormal 138

Fig. 7. Segmentation results of 11 selected cervical cell images from (a) to (k), where the left images are the originals and the right images show the segmented results.

The segmentation results, as displayed in Fig. 7, generally demonstrate the ability of the segmentation algorithm to focus on the nucleus region, which is critical for cervical cell analysis. Since the nucleus plays a significant role in distinguishing normal and abnormal cells, the primary evaluation question is how effectively the segmentation isolates and captures the nucleus across various images. Images (a) - (d) feature relatively smaller nuclei, while images (e) - (g) exhibit medium-sized nuclei, and images (h) – (k) display larger nuclei compared to the others.

A closer look at the black-and-white segmentation masks shows that the segmentation results generally follow the proportional size and shape of the nuclei across different samples. For instance, in images (a) – (d), the segmented nucleus appears smaller, aligning with the actual nucleus size in the corresponding original images. Similarly, images (h) – (k), which have larger nuclei, display proportionately larger segmented masks. This indicates that the segmentation method effectively adapts to different nucleus sizes, maintaining the proportionality and relative boundaries.

However, there are also some observed limitations in the segmentation. Notably, in image (d), the segmentation includes additional noise, resulting in a less refined boundary around the nucleus. This could potentially affect classification accuracy if such noise remains uncorrected in preprocessing. Furthermore, image 10 presents an interesting segmentation inversion, where the nucleus becomes part of the background (black), and the cytoplasm is segmented as the primary object (white). This inversion may reflect an edge case where the algorithm misinterprets intensity levels, leading to inaccurate segmentation.

Despite these occasional anomalies, the segmentation results are, overall, relatively acceptable, capturing the key morphological features of the cervical cell nuclei in most samples. These observations suggest that the segmentation technique successfully generates binary masks that align well with the nuclei's actual

Manuscript received March 20, 2025; Accepted May 12, 2025; date of publication May 20, 2025
Digital Object Identifier (**DOI**): https://doi.org/10.35882/jeeemi.v7i2.652

dimensions in a majority of the cases. However, given that this study's primary focus is on image classification, no quantitative evaluation of segmentation accuracy was performed in this section. Instead, the segmented masks were visually assessed to ensure that they provide sufficiently accurate input for subsequent classification.

To present the classification performance clearly, the confusion matrices for each model are illustrated in Fig. 8, Fig. 9, and Fig. 10. These figures show the detailed outcomes of the classification process, highlighting the number of correctly and incorrectly classified instances for normal and abnormal cervical cells. Specifically, Fig. 8 represents the confusion matrix for the CNN model, which achieved the highest overall accuracy and precision. Fig. 9 displays the confusion matrix for the SVM model, illustrating moderate performance with a relatively higher tendency for false negatives. Finally, Fig. 10 shows the confusion matrix for the KNN model, which, while achieving lower accuracy compared to CNN and SVM, still demonstrates reasonable classification capability.

		Predicted	
		Normal	Abnormal
Actual	Normal	203	42
	Abnormal	31	641

Fig. 8. Confusion Matrix of CNN

		Predicted	
		Normal	Abnormal
Actual	Normal	165	81
	Abnormal	31	640

Fig. 9. Confusion matrix of SVM

		Predicted	
		Normal	Abnormal
Actual	Normal	161	69
	Abnormal	72	615

Fig. 10. Confusion matrix of KNN

The CNN model demonstrated the strongest performance among the three classifiers in terms of accuracy, precision, and sensitivity. With an accuracy of 85%, CNN correctly classified 779 out of 917 images, achieving the highest overall classification rate. The precision of 86.70% indicates that CNN can confidently predict abnormal cervical cells with a low false positive rate, minimizing unnecessary alerts and follow-ups. Additionally, its sensitivity of 83% shows that it can detect 83% of actual abnormal cases while missing 17% due to false negatives. This balance between precision and sensitivity makes CNN highly reliable for medical diagnostics, where detecting abnormalities while minimizing false positives is crucial for patient outcomes.

The SVM classifier had moderate performance compared to CNN, with an accuracy of 78.95%. It achieved an 84% precision, meaning that most abnormal predictions were correct, which is important in minimizing false positives. However, its sensitivity was relatively low at 67%, indicating that the SVM struggled to detect abnormal cases effectively and missed a significant number of them. This trade-off between high precision and lower recall means that while SVM can accurately classify abnormal cells, it may overlook many true abnormal cases, leading to potential risks in clinical diagnostics. This performance imbalance suggests that SVM could benefit from enhanced feature selection, hyperparameter tuning, or being part of an ensemble method to improve recall without sacrificing precision.

The KNN model performed the weakest among the three classifiers, with an accuracy of 72.90%. Despite achieving a high precision of 69.23%, its sensitivity was low at 70%, reflecting a significant challenge in correctly identifying abnormal cervical cells. This low sensitivity indicates that KNN frequently misclassifies abnormal cases as normal, resulting in 30% of actual abnormal cases being missed. Additionally, KNN's performance may be affected by its inherent sensitivity to noisy data and its reliance on simple distance-based metrics. In

Manuscript received March 20, 2025; Accepted May 12, 2025; date of publication May 20, 2025
Digital Object Identifier (**DOI**): https://doi.org/10.35882/jeeemi.v7i2.652

medical diagnostics, this low recall is a significant concern as it could lead to missed detections of critical cases, underscoring the need for further optimization or a more advanced feature representation.

Table 5. Performance of classification

Classifier	Accuracy (%)	Precision (%)	Sensitivity (%)
CNN	85	86.07	83
SVM	78.95	84	67
KNN	72.90	86.70	70

This section presents analysis of the accuracy, precision, and sensitivity of cervical cell classification methods. The research seeks to determine the most efficient approach for classifying cervical cell images by training and testing on a dataset of 917 images, with 80% used for training and 20% for testing. According to the results depicted in Table 5 and Fig. 11, the CNN outperforms other methods, achieving an accuracy of 85%, higher than the SVM at 78.95% and KNN at 72.8%. Precision, measuring positive predictions' accuracy, is crucial in healthcare; CNN exhibits 86.7%, surpassing SVM (84%) and KNN (69.23%). Sensitivity, gauging the ability to identify abnormal cases, sees CNN leading with 83%, outperforming SVM (67%) and KNN (70%). in accurately classifying cervical cell images.

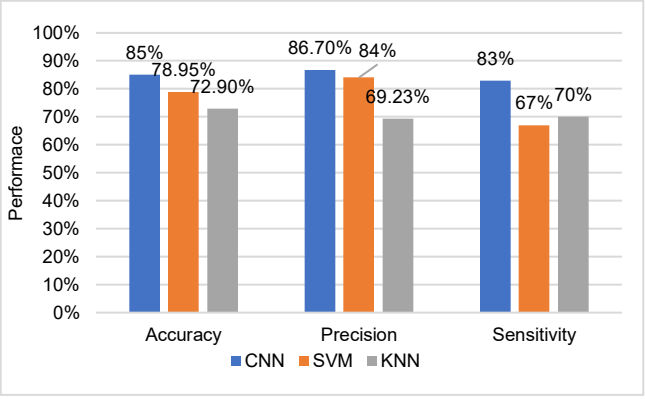

Fig. 11. Visual representation of classification performance

4. Discussion

All three classifiers exhibit distinct strengths and weaknesses, CNN outperformed both SVM and KNN in terms of accuracy, precision, and recall, making it the most balanced and effective model for cervical cell classification. SVM's high precision but low recall suggests that it excels in avoiding false positives but struggles to capture true abnormal cases. KNN, with its weaker overall performance, highlights the importance of optimizing distance-based classification in noisy medical datasets. To further enhance classification performance, future work could explore ensemble techniques, deeper hyperparameter tuning, or advanced feature extraction methods to strike a better balance between precision and recall across all models.

In comparison to previous studies, the CNN-based classifier implemented in this study demonstrates competitive performance. For instance, Wu et al. [16] achieved a classification accuracy of 99.5% using a hybrid CNN-LSVM model optimized with Adaboost, but their method involved a more complex ensemble framework with higher computational requirements. Notably, Wu et al.'s study focused on binary classification, which generally tends to yield higher accuracy compared to multi-class problems. Similarly, Ghoneim et al. [19] reported an accuracy of 99.5% using a CNN-ELM ensemble, which, while effective, combines both deep and shallow learners and also addresses a binary classification task. In contrast, the CNN in this study, though achieving a lower accuracy of 85%, is a lightweight standalone model that is computationally simpler and better suited for resource-constrained environments. Compared to the RES_DCGAN-ResNet50V2 model used by Wubineh et al. [13], which enhances performance through data augmentation and self-attention mechanisms, our approach focuses on conventional preprocessing and handcrafted features, reflecting a more accessible implementation. These comparisons highlight that while our CNN approach may not outperform deep ensemble models designed for binary classification, it offers a favorable trade-off between accuracy, simplicity, and computational efficiency, making it suitable for practical cervical cancer screening applications.

Despite the models demonstrating varying degrees of success in cervical cell classification, this study has several limitations that impact its overall reliability and practical applicability. One of the main concerns lies in the dataset imbalance, as the Herlev dataset contains more abnormal cells than normal cells, potentially skewing the classifier's learning process and leading to biased predictions. Additionally, the absence of rigorous hyperparameter tuning and advanced preprocessing techniques may have affected the models' performance, particularly for SVM and KNN, which are more sensitive to feature scaling and input data variability. Furthermore, the segmentation process, although visually acceptable in most cases, occasionally misidentifies nuclei boundaries or includes noise, reducing the quality of input features and affecting downstream classification performance. The lack of numerical metrics for segmentation evaluation and the exclusive reliance on classification metrics also weaken the overall depth of the study, making it difficult to comprehensively assess

Manuscript received March 20, 2025; Accepted May 12, 2025; date of publication May 20, 2025
Digital Object Identifier (**DOI**): https://doi.org/10.35882/jeeemi.v7i2.652

how segmentation errors propagate through the classification process. These limitations highlight the need for further refinement in both the preprocessing pipeline and the choice of classification approaches to enhance the robustness and accuracy of future cervical cell classification systems.

From a practical standpoint, the findings of this study hold promising implications for integrating automated cervical cell classification into clinical workflows. The CNN-based model, despite its lower accuracy compared to more complex ensemble methods, is computationally lightweight and easier to deploy, making it particularly suitable for use in low-resource settings such as rural clinics or mobile screening units where high-end hardware and internet connectivity may be limited. Its simplicity also supports faster inference times, allowing for real-time or near-real-time diagnostic assistance during cytological examinations. Integrating such a model into digital pathology systems or microscope-based image acquisition tools could assist cytotechnologists by pre-screening slides and highlighting potential abnormal regions, thereby reducing workload and improving early detection rates. For future implementation strategies, collaboration with healthcare professionals will be essential to ensure the model aligns with clinical requirements, such as interpretability, integration with electronic health records, and compliance with medical device regulations. Additionally, further validation on larger, more diverse datasets and the development of user-friendly interfaces will be necessary steps to move from experimental research toward practical deployment in cervical cancer screening programs.

5. Conclusion

This study aims to classify cervical cell images using Artificial Intelligence (AI) techniques by comparing the performance of Convolutional Neural Networks (CNN), Support Vector Machines (SVM), and K-Nearest Neighbors (KNN). Among the three classifiers, CNN achieved the best overall performance, with an accuracy of 85%, precision of 86.7%, and sensitivity of 83%, indicating its strong potential for cervical cell classification tasks. These results suggest that supervised classification methods are more effective than unsupervised approaches in this domain, likely due to their ability to learn complex patterns from labeled data. Additionally, the lightweight CNN model used in this study offers a favorable balance between accuracy and computational simplicity, making it more suitable for deployment in resource-constrained clinical settings.

However, class imbalance in the Herlev dataset remains a challenge, as it can bias model predictions and reduce generalizability. To address this, future work should explore data balancing techniques such as Generative Adversarial Networks (GANs) for synthetic sample generation or data augmentation strategies to enrich underrepresented classes. Further improvements could also involve hyperparameter optimization, advanced feature selection, and ensemble learning methods to boost performance across multiple evaluation metrics. Ultimately, expanding the dataset and validating the model in real clinical scenarios will be essential for translating these findings into practical cervical cancer screening solutions.

Acknowledgment

This research was supported by funding from the Ministry of Higher Education (MoHE) Malaysia under the Fundamental Research Grant Scheme (FRGS/1/2021/SKK0/UNIMAP/02/1).

.

References

[1] World Health Organization, “Cervical cancer,” Geneva, Mar. 05, 2024.

[2] A. Petca, A. Borislavschi, M. Zvanca, R.-C. Petca, F. Sandru, and M. Dumitrascu, “Non-sexual HPV transmission and role of vaccination for a better future (Review),” *Exp Ther Med*, vol. 20, no. 6, 2020, doi: 10.3892/etm.2020.9316.

[3] K. S. Okunade, “Human papillomavirus and cervical cancer,” *J Obstet Gynaecol (Lahore)*, vol. 40, no. 5, pp. 602–608, 2020, doi: 10.1080/01443615.2019.1634030.

[4] W. A. Mustafa, S. Ismail, F. S. Mokhtar, H. Alquran, and Y. Al-Issa, “Cervical Cancer Detection Techniques: A Chronological Review,” 2023. doi: 10.3390/diagnostics13101763.

[5] H. Bandyopadhyay and M. Nasipuri, “Segmentation of Pap Smear Images for Cervical Cancer Detection,” *2020 IEEE Calcutta Conference, CALCON 2020 - Proceedings*, pp. 30–33, Feb. 2020, doi: 10.1109/CALCON49167.2020.9106484.

[6] M. I. Waly, M. Y. Sikkandar, M. A. Aboamer, S. Kadry, and O. Thinnukool, “Optimal deep convolution neural network for cervical cancer diagnosis model,” *Computers, Materials and Continua*, vol. 70, no. 2, 2022, doi: 10.32604/cmc.2022.020713.

[7] W. A. Mustafa, A. Halim, M. W. Nasrudin, and K. S. A. Rahman, “Cervical cancer situation in Malaysia: A systematic literature review,” 2022. doi: 10.32604/biocell.2022.016814.

[8] T. Vaiyapuri *et al.*, “Modified metaheuristics with stacked sparse denoising autoencoder model for cervical cancer classification,” *Computers and*

Manuscript received March 20, 2025; Accepted May 12, 2025; date of publication May 20, 2025
Digital Object Identifier (**DOI**): https://doi.org/10.35882/jeeemi.v7i2.652

Electrical Engineering, vol. 103, 2022, doi: 10.1016/j.compeleceng.2022.108292.

[9] K. Prasad Battula and B. S. Chandana, "Deep Learning based Cervical Cancer Classification and Segmentation from Pap Smears Images using an EfficientNet," 2022. [Online]. Available: www.ijacsa.thesai.org

[10] A. Rasheed, S. H. Shirazi, A. I. Umar, M. Shahzad, W. Yousaf, and Z. Khan, "Cervical cell's nucleus segmentation through an improved UNet architecture," *PLoS One*, vol. 18, no. 10 October, 2023, doi: 10.1371/journal.pone.0283568.

[11] E. Zhang *et al.*, "Cervical cell nuclei segmentation based on GC-UNet," *Heliyon*, vol. 9, no. 7, p. e17647, Jul. 2023, doi: 10.1016/J.HELIYON.2023.E17647.

[12] M. M. Rahaman *et al.*, "DeepCervix: A deep learning-based framework for the classification of cervical cells using hybrid deep feature fusion techniques," *Comput Biol Med*, vol. 136, p. 104649, Sep. 2021, doi: 10.1016/J.COMPBIOMED.2021.104649.

[13] B. Z. Wubineh, A. Rusiecki, and K. Halawa, "Classification of cervical cells from the Pap smear image using the RES_DCGAN data augmentation and ResNet50V2 with self-attention architecture," *Neural Comput Appl*, vol. 36, no. 34, pp. 21801–21815, Dec. 2024, doi: 10.1007/S00521-024-10404-X/FIGURES/8.

[14] C. W. Zhang, D. Y. Jia, N. K. Wu, Z. G. Guo, and H. R. Ge, "Quantitative detection of cervical cancer based on time series information from smear images," *Appl Soft Comput*, vol. 112, p. 107791, Nov. 2021, doi: 10.1016/J.ASOC.2021.107791.

[15] L. Nanni, S. Ghidoni, S. Brahnam, S. Liu, and L. Zhang, "Ensemble of handcrafted and deep learned features for cervical cell classification," *Intelligent Systems Reference Library*, vol. 186, pp. 117–135, 2020, doi: 10.1007/978-3-030-42750-4_4.

[16] N. Wu, D. Jia, C. Zhang, and Z. Li, "Cervical cell classification based on strong feature CNN-LSVM network using Adaboost optimization," *Journal of Intelligent and Fuzzy Systems*, vol. 44, no. 3, pp. 4335–4355, 2023, doi: 10.3233/JIFS-221604.

[17] H. Alquran, W. Azani Mustafa, F. F. Mohammed, and A. Alkhayyat, "Nucleus Detection Using Deep Learning Approach on Pap Smear Images," in *2023 6th International Conference on Engineering Technology and its Applications (IICETA)*, IEEE, Jul. 2023, pp. 665–668. doi: 10.1109/IICETA57613.2023.10351221.

[18] W. A. Mustafa, L. Z. Wei, and K. S. Ab Rahman, "Automated cell nuclei segmentation on cervical smear images using structure analysis," *Journal of Biomimetics, Biomaterials and Biomedical Engineering*, vol. 51, 2021, doi: 10.4028/www.scientific.net/JBBBE.51.105.

[19] A. Ghoneim, G. Muhammad, and M. S. Hossain, "Cervical cancer classification using convolutional neural networks and extreme learning machines," *Future Generation Computer Systems*, vol. 102, pp. 643–649, Jan. 2020, doi: 10.1016/J.FUTURE.2019.09.015.

[20] T. Conceição, C. Braga, L. Rosado, and M. J. M. Vasconcelos, "A Review of Computational Methods for Cervical Cells Segmentation and Abnormality Classification," *International Journal of Molecular Sciences 2019, Vol. 20, Page 5114*, vol. 20, no. 20, p. 5114, Oct. 2019, doi: 10.3390/IJMS20205114.

[21] A. Mohammed and R. Kora, "A comprehensive review on ensemble deep learning: Opportunities and challenges," *Journal of King Saud University - Computer and Information Sciences*, vol. 35, no. 2, pp. 757–774, Feb. 2023, doi: 10.1016/J.JKSUCI.2023.01.014.

[22] I. Mansoury, D. El Bourakadi, A. Yahyaouy, and J. Boumhidi, "Optimized extreme learning machine using genetic algorithm for short-term wind power prediction," *Bulletin of Electrical Engineering and Informatics*, vol. 13, no. 2, pp. 1334–1343, Apr. 2024, doi: 10.11591/EEI.V13I2.6476.

[23] H. Wei *et al.*, "A texture feature extraction method considering spatial continuity and gray diversity," *International Journal of Applied Earth Observation and Geoinformation*, vol. 130, p. 103896, Jun. 2024, doi: 10.1016/J.JAG.2024.103896.

[24] I. Chaabane, R. Guermazi, and M. Hammami, "Enhancing techniques for learning decision trees from imbalanced data," *Adv Data Anal Classif*, vol. 14, no. 3, pp. 677–745, Sep. 2020, doi: 10.1007/S11634-019-00354-X/TABLES/19.

[25] E. Gokgoz and A. Subasi, "Comparison of decision tree algorithms for EMG signal classification using DWT," *Biomed Signal Process Control*, vol. 18, 2015, doi: 10.1016/j.bspc.2014.12.005.

[26] V. K. Chandu, B. K. Sairam, and S. J. Prakash, "Cervical Cancer Cell Detection Using Image Processing and Matlab," 2024.

[27] P. Wang, L. Wang, Y. Li, Q. Song, S. Lv, and X. Hu, "Automatic cell nuclei segmentation and classification of cervical Pap smear images," *Biomed Signal Process Control*, vol. 48, pp. 93–103, Feb. 2019, doi: 10.1016/J.BSPC.2018.09.008.

[28] N. B. Byju, • Vilayil, K. Sujathan, P. Malm, and • R Rajesh Kumar, "A fast and reliable approach to

Manuscript received March 20, 2025; Accepted May 12, 2025; date of publication May 20, 2025
Digital Object Identifier (**DOI**): https://doi.org/10.35882/jeeemi.v7i2.652

cell nuclei segmentation in PAP stained cervical smears," *CSI Transactions on ICT 2013 1:4*, vol. 1, no. 4, pp. 309–315, Oct. 2013, doi: 10.1007/S40012-013-0028-Y.

[29] L. Sukel and L. Sukesh, "Detection of Cervical Cancer Using Gaussian Filter and Canny Edge Detection Algorithm," *International Research Journal of Engineering and Technology*, vol. 7209, 2008, doi: 10.1128/CMR.16.1.1-17.

[30] R. C. Gonzalez, R. E. Woods, and B. R. Masters, "Digital Image Processing, Third Edition," *J Biomed Opt*, vol. 14, no. 2, 2009, doi: 10.1117/1.3115362.

[31] C. Bergmeir, M. García Silvente, and J. M. Benítez, "Segmentation of cervical cell nuclei in high-resolution microscopic images: A new algorithm and a web-based software framework," *Comput Methods Programs Biomed*, vol. 107, no. 3, pp. 497–512, Sep. 2012, doi: 10.1016/J.CMPB.2011.09.017.

[32] P. Bamford and B. Lovell, "Unsupervised cell nucleus segmentation with active contours," *Signal Processing*, vol. 71, no. 2, pp. 203–213, Dec. 1998, doi: 10.1016/S0165-1684(98)00145-5.

[33] P. Cunningham and S. J. Delany, "k-Nearest Neighbour Classifiers: 2nd Edition (with Python examples)," *ACM Comput Surv*, vol. 54, no. 6, Apr. 2020, doi: 10.1145/3459665.

[34] P. K. Syriopoulos, N. G. Kalampalikis, S. B. Kotsiantis, and M. N. Vrahatis, "kNN Classification: a review," *Ann Math Artif Intell*, pp. 1–33, Sep. 2023, doi: 10.1007/S10472-023-09882-X/METRICS.

[35] R. O. Duda, P. E. Hart, and D. G. Stork, "Pattern Classification (2nd ed .)," *Computational Complexity*, 1998.

[36] S. Suthaharan, "Machine Learning Models and Algorithms for Big Data Classification," vol. 36, 2016, doi: 10.1007/978-1-4899-7641-3.

[37] M. Khorshid, T. H. M. Abou-El-Enien, and G. M. A. Soliman, "A Comparison among Support Vector Machine and other Machine Learning Classification Algorithms," 2015.

[38] S. Abe, "Support Vector Machines for Pattern Classification," 2010, doi: 10.1007/978-1-84996-098-4.

[39] A. K. Jain, R. P. W. Duin, and J. Mao, "Statistical pattern recognition: A review," *IEEE Trans Pattern Anal Mach Intell*, vol. 22, no. 1, pp. 4–37, Jan. 2000, doi: 10.1109/34.824819.

[40] M. Awad and R. Khanna, "Support Vector Machines for Classification," *Efficient Learning Machines*, pp. 39–66, 2015, doi: 10.1007/978-1-4302-5990-9_3.

[41] K. O'Shea and R. Nash, "An Introduction to Convolutional Neural Networks," *Int J Res Appl Sci Eng Technol*, vol. 10, no. 12, pp. 943–947, Nov. 2015, doi: 10.22214/ijraset.2022.47789.

[42] X. Zhao, L. Wang, Y. Zhang, X. Han, M. Deveci, and M. Parmar, "A review of convolutional neural networks in computer vision," *Artif Intell Rev*, vol. 57, no. 4, pp. 1–43, Apr. 2024, doi: 10.1007/S10462-024-10721-6/FIGURES/33.

[43] A. Khan, A. Sohail, U. Zahoora, and A. S. Qureshi, "A survey of the recent architectures of deep convolutional neural networks," *Artificial Intelligence Review 2020 53:8*, vol. 53, no. 8, pp. 5455–5516, Apr. 2020, doi: 10.1007/S10462-020-09825-6.

[44] Z. Zheng, Z. Chen, F. Hu, J. Zhu, Q. Tang, and Y. Liang, "An automatic diagnosis of arrhythmias using a combination of CNN and LSTM technology," *Electronics (Switzerland)*, vol. 9, no. 1, 2020, doi: 10.3390/electronics9010121.

[45] A. Desiani, M. Erwin, B. Suprihatin, S. Yahdin, A. I. Putri, and F. R. Husein, "Bi-path Architecture of CNN Segmentation and Classification Method for Cervical Cancer Disorders Based on Pap-smear Images," *IAENG Int J Comput Sci*, vol. 48, no. 3, 2021.

Manuscript received March 20, 2025; Accepted May 12, 2025; date of publication May 20, 2025
Digital Object Identifier (**DOI**): https://doi.org/10.35882/jeeemi.v7i2.652

Author Biography

WAN AZANI MUSTAFA is a senior lecturer at Universiti Malaysia Perlis (UniMAP) and a research fellow at the Center of Excellence for Advanced Computing, UniMAP. He obtained his Ph.D. in Mechatronic Engineering in 2017 and his degree in Biomedical Electronic Engineering in 2013, both from UniMAP. He is a member of the Board of Engineers Malaysia (BEM, since 2014) and the Malaysia Board of Technologists (MBOT, since 2017) and holds the status of Senior Member of IEEE. His current research interests include image processing, biomechanics, intelligent systems, and computer science. Dr. Wan Azani has published several articles in reputable journals such as MDPI, Tech Science, and Elsevier. His Scopus metrics include 265 citations and an H-index of 16, while his Google Scholar metrics record 310 citations and an H-index of 18.

Contact details:
Faculty of Electrical Engineering & Technology,
Universiti Malaysia Perlis, Pauh Putra Campus, 02600 Arau, Perlis, Malaysia
Phone: +60133003401
E-mail: wanazani@unimap.edu.my

KHALIS DANIAL NUKMAN KHIRUDDIN was born in Perak, Malaysia. He holds a Bachelor's Degree in Biomedical Electronic Engineering, graduating with first-class honors in 2023. Currently, he is a Graduate Research Assistant in the Faculty of Electrical Engineering and Technology at the University Malaysia Perlis, where he is pursuing a Master's degree in Mechatronic Engineering, focusing on medical image and signal processing, with a minor involvement in deep learning. He has accumulated a range of experiences, including roles as a teacher, tutor, and freelancing undergraduate final year project mentor. Additionally, he has gained industry experience through an internship on the production line at CCB Medical Devices SDN BHD. Awarded for his academic excellence, Khalis is a recipient of the prestigious Jasso Scholarship, which enabled him to participate in an exchange program at the University of Yamanashi in Japan. His research interests lie in the fields of image and signal processing, medical imaging, and deep learning. Registered as a Graduate Engineer with the Board of Engineering Malaysia, Mr. Khalis has also actively contributed to the community through his involvement in STEM workshops and classes in rural area schools. These experiences highlight his dedication to both professional development and community engagement.

KHAIRUR RIJAL JAMALUDIN is a distinguished professor at the Faculty of Artificial Intelligence, Universiti Teknologi Malaysia (UTM), specializing in materials science, powder metallurgy, metal injection molding, manufacturing process mechanics, and quality management. With 175 publications, including 100 indexed papers, his research has garnered 902 citations and an H-index of 16 on Scopus. He has led and contributed to 43 research grants and supervised 77 postgraduate students. His expertise spans advanced manufacturing techniques, lean production, the Mahalanobis Taguchi System, and remanufacturing. Through his extensive academic and industrial collaborations, he continues to drive innovation in artificial intelligence applications within manufacturing and materials processing. He can be reached at *khairur.kl@utm.my*.

MUHAMMAD FIRDAUS YUSLAN KHUSAIRI, hailing from Semenyih, Selangor, Malaysia, is an aspiring engineer with a strong background in mechatronics and electrical engineering. He began his academic journey by earning a Diploma in Vocational Mechatronic Engineering from the Malaysian Institute of Technology Academy.

Building upon his technical foundation, he pursued a Bachelor's Degree in Electrical Engineering Technology (Hons.) with a specialization in Robotic & Automation Technology at Universiti Malaysia Perlis (UniMAP). His passion for automation and robotics has driven him to gain hands-on experience in the industry.

During his academic tenure, Muhammad Firdaus undertook industrial training at Infineon Technologies Kulim Sdn. Bhd., where he honed his practical skills in semiconductor manufacturing and automation systems. His experience in this global technology company has provided him with invaluable insights into the industry's cutting-edge advancements.).

Manuscript received March 20, 2025; Accepted May 12, 2025; date of publication May 20, 2025
Digital Object Identifier (**DOI**): https://doi.org/10.35882/jeeemi.v7i2.652

SHAHRINA ISMAIL is a senior lecturer at the Faculty of Science and Technology, Universiti Sains Islam Malaysia (USIM). She earned her Ph.D. in Mathematics from the University of Queensland, Brisbane, Australia, in 2017, specializing in pure mathematics. Her expertise extends to qualitative and quantitative studies, financial mathematics, and STEM education. An active researcher, she has secured multiple grants, including the Fundamental Research Grant Scheme (FRGS), USIM Racer Grant, and DSRG under MCMC. These grants support her work in advancing mathematical applications and interdisciplinary studies. Beyond academia, Shahrina is dedicated to promoting STEM education. As the founder of the "Maths is Fun" program, she visits schools to make mathematics more engaging for students. Through interactive sessions, she fosters a deeper appreciation for the subject and encourages STEM participation. Committed to research and education, she welcomes collaboration and can be reached at shahrinaismail@usim.edu.my.

Manuscript received March 20, 2025; Accepted May 12, 2025; date of publication May 20, 2025
Digital Object Identifier (**DOI**): https://doi.org/10.35882/jeeemi.v7i2.652